MIT Open Access Articles

Melt-driven mechanochemical phase transformations in moderately exothermic powder mixtures

Melt-driven mechanochemical phase transformations in moderately exothermic powder mixtures

Samuel A. Humphry-Baker*[1,2], Sebastiano Garroni[3], Francesco Delogu[4] and Christopher A. Schuh[1]

[1]*Department of Materials Science and Engineering, Massachusetts Institute of Technology, Cambridge, MA 02139, USA*
[2]*Department of Materials, Imperial College, London SW7 2AZ, UK*
[3]*Dipartimento di Chimica e Farmacia, Università degli Studi di Sassari, via Vienna 2, 07100 Sassari, Italy*
[4]*Dipartimento di Ingegneria Meccanica, Chimica e dei Materiali, Università degli Studi di Cagliari, via Marengo 2, 09123 Cagliari, Italy*

Abstract

Usually, mechanochemical reactions between solid phases are either gradual (by deformation-induced mixing), or self-propagating (by exothermic chemical reaction). Here, by means of a systematic kinetic analysis of the Bi-Te system reacting to Bi_2Te_3, we establish a third possibility: if one or more of the powder reactants has a low melting point and low thermal effusivity, it is possible that local melting can occur from deformation-induced heating. The presence of hot liquid then triggers chemical mixing locally. The molten events are constrained to individual particles, making them distinct from self-propagating reactions, and occur much faster than conventional gradual reactions. We show that the mechanism is applicable to a broad variety of materials systems, many of which have important functional properties. This mechanistic picture offers a new perspective as compared to conventional, gradual mechanochemical synthesis, where thermal effects are generally ignored.

* Corresponding author email: shumphry@ic.ac.uk

Mechanical stress and strain can substantially affect chemical reactions, as in selective activation of covalent systems[1,2], wear-induced chemical reactions[3,4], or mechanochemically-induced unusual reactivity in solids[5–8]. Mechanochemical processing benefits from lower temperatures, reduced use of chemical solvents, and fewer processing steps than traditional synthesis routes[9]. Typically, mechanochemical processing involves powdered materials being milled, i.e., repeatedly forged, fractured, and re-welded under high-strain rates[5], leading to nonequilibrium reactions to unique compounds and microstructures[10–12].

The nonequilibrium, or "driven", character of mechanical processing is generally assumed to be predominantly athermal, tending to homogenize the chemical composition rather than the chemical potential, as favoured by thermodynamic equilibrium[13–15]. The competition between these two tendencies forms the basis of driven systems theory[16], and can explain why, e.g., immiscible alloy systems often form solid solutions during milling[13,14]; if the rate of ballistic mixing exceeds the rate of chemical diffusion and phase separation then mixing will occur[16]. Such driven reactions occur gradually over an extended period of time, e.g. several hours, as mechanical work is spread throughout the solid particles.

A simple diffusive-vs-ballistic mixing framework cannot explain all mechanochemical reactions however[17–20]; in some cases, local temperature rise plays a role[21–23]. Mechanically induced self-propagating reactions (MSRs) are aided by the thermal energy from bond formation between dissimilar atoms; when two reactive species are mechanically ground together, the negative enthalpy of their mixing is released instantaneously, resulting in an autocatalytic propagation of the reaction[24,25]. During ball milling, MSRs are ignited spontaneously once the structure reaches a critical level of forced mixing, after which the reaction tends to consume the entire powder charge in an instantaneous manner.

Thus, two dominant types of driven reactions have been demonstrated: the gradual reactions promoted by mechanical energy input, and the abrupt MSRs promoted by the chemical

2

energy of the exothermic reaction. In this paper we provide evidence for a third type of mechanochemical reaction, which exhibits some characteristics of the above two, but which is physically distinct and may have broad implications for low thermal effusivity materials of interest in energy and heat management applications. Specifically, we show that for at least some systems, the heating caused by mechanical work can lead to localized melting that in turn triggers local chemical reaction. The resulting new class of mechanochemical reactions provides some clarity on the controversial topic of contact melting in driven systems.

Impact characterization

The first step of our analysis involves quantitative microscopy of phase formation after a single mechanochemical unit process: a single impact of powder particles by tooling. Impact tests were performed on powders of elemental Bi and Te mixed in a molar ratio of 2:3, using a SPEX 8000 mixer mill (see methods). Fig. 1a shows a representative collision, imaged in a scanning electron microscope, in which perhaps a few hundred reactant powder particles of pure Bi and Te were flattened by the impact of a single 8 g steel ball. The resultant cold-welded compacts had an average measured impact radius of 680 μm and estimated thickness of 100 μm[26]. The reactant powder particles have reacted over a considerable scale, with a high volume fraction of product (intermetallic Bi_2Te_3) phase of about $f = 0.25$. The extent of phase formation is quantified in part (b), which shows the cumulative distribution of Bi_2Te_3 phase in 23 stereologically measured compacts. The average product volume fraction is $f = 0.14$.

The reaction morphology in Fig. 1 exhibits alloyed regions localized within bands that originate at the center of the compact and radiate outwards. We call such a localized event a critical loading condition (CLC). A CLC event is revealed in more detail in Fig. 1c, which shows the central region of the compact at higher magnification, where the components

3

appear to have melted and flowed as a liquid (Fig. 1c). What is more, close inspection of locations where such bands reach the periphery of the compact reveals ejected material containing droplets (Fig. 1d) and rounded splash marks (Fig. 1e). Such observations strongly speak to the presence of liquid phase, and we deduce that the mechanical energy has induced
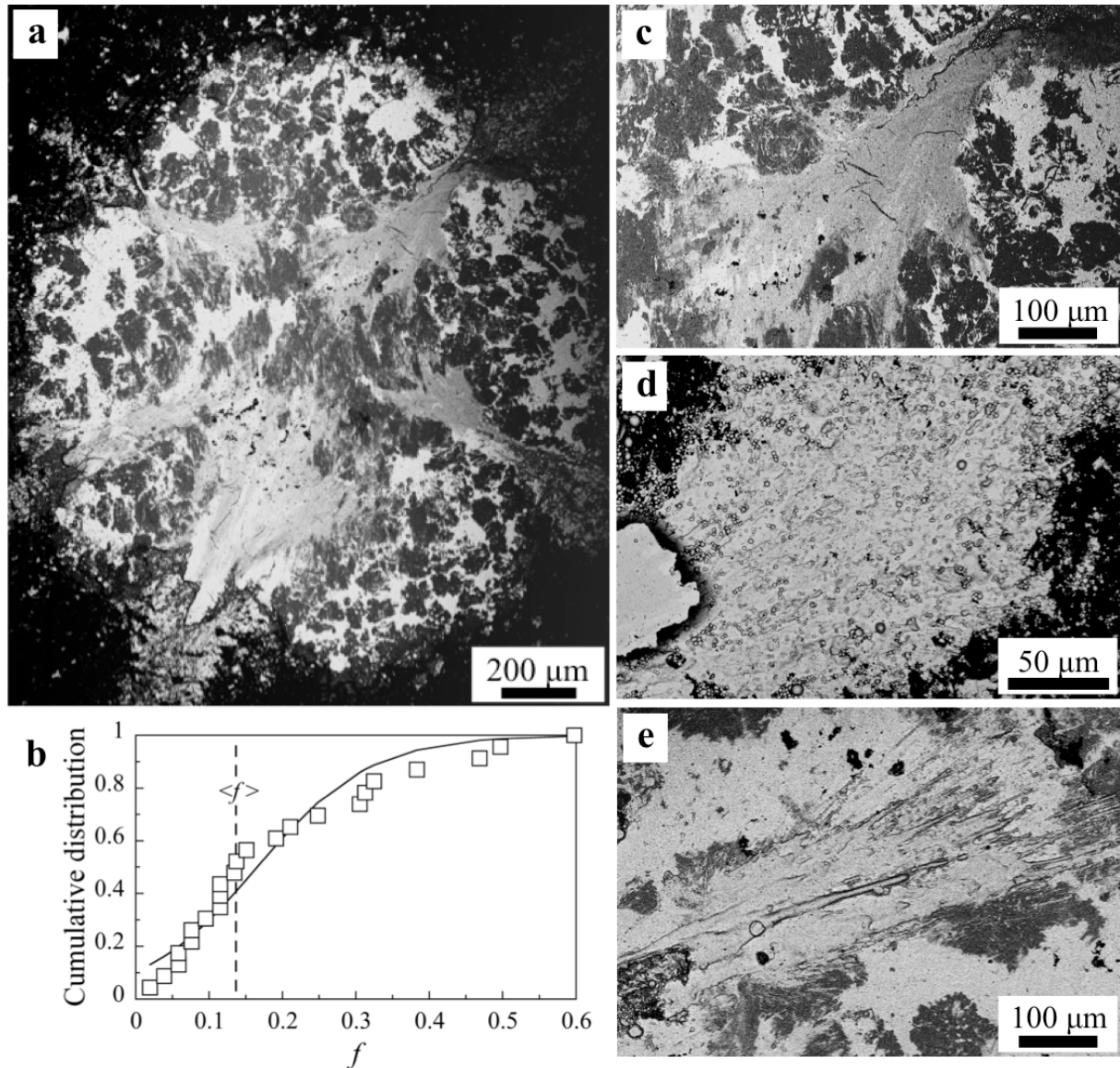
melting through adiabatic heating.

Figure 1 | Bi melts locally under impact. a, an SEM image of a typical compact, showing the geometry of intermetallic formation during a typical collision. Bi regions appear white, Te black, and Bi_2Te_3 grey. **b**, the cumulative distribution of intermetallic volume fractions from 23 compacts. **c-e**, magnified images of a CLC event: **c**, flow of liquid Bi around Te particles; **d**, ejection of liquid Bi at the compact edge; and **e**, splash marks from liquid Bi.

Based on this evidence we propose that molten Bi is first formed at the compact center once a critical amount of deformation is reached. Similar observations of deformation-induced melting have been made, e.g. during high-strain rate deformation of metallic glasses, thus melting a Sn surface coating[27], or during high speed frictional loading on metallic surfaces, e.g. Pb, Sn, and Bi[28]. Indeed, contact melting during mechanical processing has been suggested theoretically[29,30] and observed in numerical simulations[31] – but not explicitly demonstrated experimentally before.

Kinetic analysis

To complement the above mechanistic observations, we now quantify the thermodynamic requirements for mechanochemical melting via systematic kinetic analysis. For this analysis, a different geometry of ball drop reactor, as schematized in Fig. 2a, was used to allow more precise control of the milling energy and temperature. However, the relevant parameters of the reactor such as the ball size, impact velocity, and ball-to-powder ratio are very similar, allowing direct comparison between experiments (see methods). Some typical X-ray diffraction (XRD) patterns of powder mixtures are shown in Fig. 2b, after about 1, 5, and 20 thousand collisions, respectively showing (i) almost exclusively reactants Bi + Te, (ii) a mixture of reactants Bi + Te and product Bi_2Te_3, and (iii) almost exclusively product Bi_2Te_3. The patterns are best-fitted using the Rietveld method, from which the volume fraction of product (Bi_2Te_3) phase, f, can be calculated. In no pattern was any angular shift of the Bi and Te XRD peaks observed, suggesting negligible mutual dissolution of Bi and Te in one another. This conforms to the idea that Bi_2Te_3 forms directly via Te dissolution in molten Bi – i.e. no phases of intermediate composition are formed – which is consistent with our SEM observations.
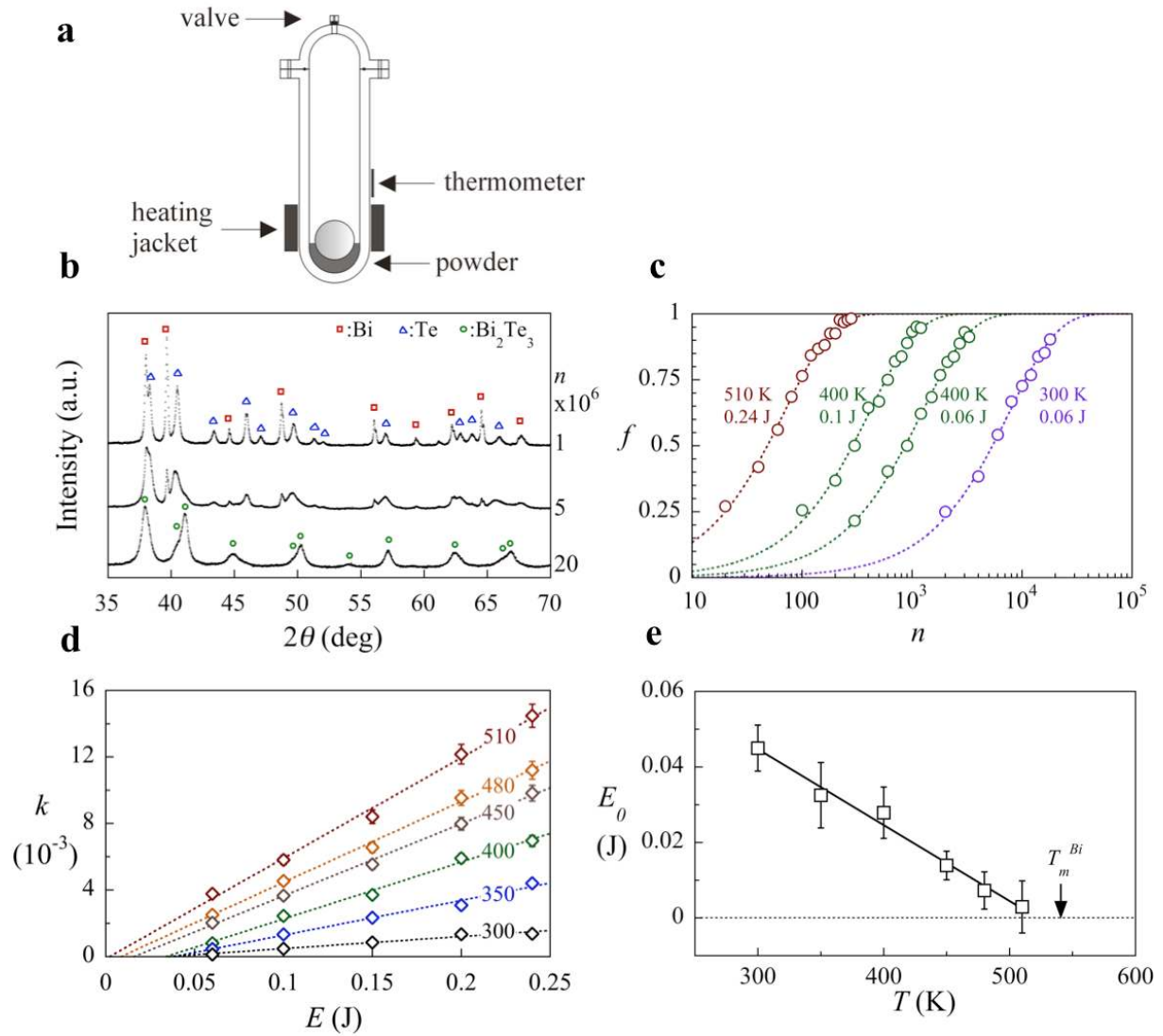
5

Figure 2 | Reaction kinetics are driven by liquid Bi. a, schematic of the ball drop reactor. **b**, raw XRD patterns, representing 3 different stages of processing. From the Rietveld analysis, the volume fraction of Bi_2Te_3 phase is plotted in **c**, fitted according to equation 1 (dotted lines). The constant of proportionality, k, from this fitting procedure is plotted in **d**, as a linear function of collision energy, E. The linear relationship can be extrapolated to $k=0$ at some finite impact energy, E_0. E_0 vanishes to zero as the milling temperature approaches the melting point of Bi, which is 544 K, as shown in **e**. Error bars in **d**,**e** indicate the standard deviation in slope.

The volume fraction of product Bi_2Te_3, f, as a function of the number of collisions, n, is plotted in Fig. 2c for a few representative datasets. In all cases, f undergoes a smooth monotonic increase, although the number of impacts required to complete the reaction varies considerably with processing conditions: between about 10^2 and 10^4. The datasets are fitted with the following kinetic equation:

$$f(n)=1-exp(-kn). \tag{1}$$

where k represents the apparent rate constant for the reaction. Equation (1) can adequately capture transformation kinetics, as shown by the good fit in Fig 2(c). The rate constant extracted from these fits, k, is related to the volume fraction of Bi_2Te_3 phase that would be formed during the first collision – i.e. in the absence of any pre-formed product phase.

Fig. 2d shows that the rate constant k increases linearly with the collision energy E at all processing temperatures. However, each line of best-fit crosses the x-axis at a finite positive collision energy value, E_0, which represents the smallest possible collision energy that gives rise to any reaction to the Bi_2Te_3 phase. We take this value of energy to be that required to initiate a CLC event in a given impact, such as those seen in Fig. 1.

As the processing temperature is increased, the rate constant increases, and E_0 decreases, suggesting that less mechanical energy is needed to activate a CLC event at higher temperatures. Fig. 2e shows the monotonic decrease in E_0 with processing temperature, T. The data can be fitted with a straight line that crosses the x-axis at a temperature of $T = 526 \pm 7$ K, which is close to the Bi melting point, $T_m^{Bi} = 544$ K. The fact that the minimum collision energy necessary to activate mixing tends to vanish as the processing temperature T approaches T_m^{Bi} supports the interpretation that Bi melting is the kinetically controlling process of the reaction. (The effect of pressure on the Bi melting point is analyzed in Supplementary Note 4, indicating that its effect can be neglected.)

We note the value of $E_0 = 0.045$ J at 300 K is about an order of magnitude larger than that typically required to induce plastic deformation during ball-milling[32]. Such values range between 0.004 J for soft FCC metals such as Cu and Ag and 0.008 J for harder BCC metals such as Fe and Ni. We can therefore assume that below E_0 plastic deformation is still induced, but that – crucially – melting of Bi is not. Thus, we can identify the excess impact energy, $E^* = (E - E_0)$, as being the energy above this threshold that is expended in melting Bi.

The transformation kinetics with respect to E^* are shown in Fig. 3. The product volume fraction is plotted against the excess energy dose, defined as $D^* = n\,E^*$, at each processing temperature. Data points taken at different impact energies become superimposed for a given temperature, forming a single curve. This indicates that for mechanochemical activation, the excess energy dose is an invariant property[33]. However, at different temperatures the curves are shifted – covering about an order of magnitude in energy dose – indicating a strong thermal component to the reaction mechanism.
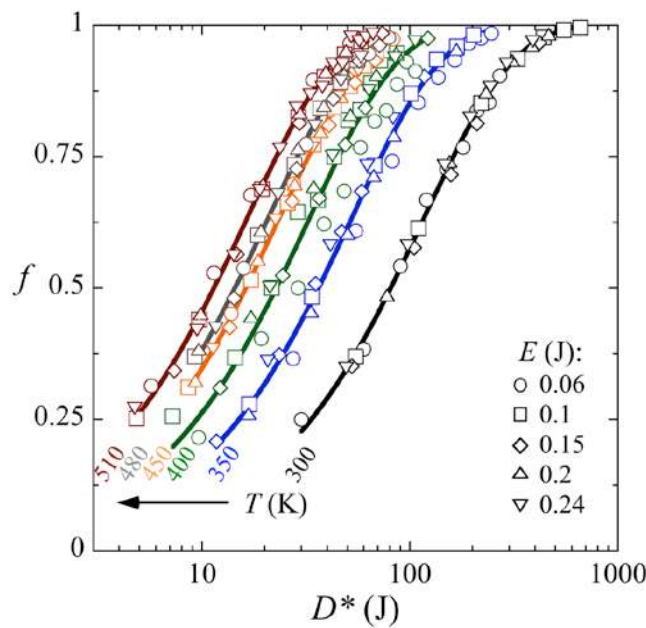

Figure 3 | There is a strong thermal component to reaction kinetics. The distinct f curves shown in Fig. 2b overlap when given as a function of the scaled dose, but are displaced with respect to the scaled dose, for a given processing temperature.

Reaction mechanism

In what follows, we seek to separate the mixing enthalpy and impact energy contributions to the reaction. We first consider the energy required to melt the quantity of Bi involved in each collision. The mass of powder converted in such an impact is simply $m^* = k\,m$, where m is the total mass of the powder charge. The minimum thermal energy required to heat this quantity

of powder from the ambient milling temperature T to the melting point of Bi, $T_m{}^{Bi}$, and then

melt it in the presence of a stoichiometric amount of Te, is:

$$E_{melt} = \frac{2m^*}{M_{Bi2Te3}} \left[\Delta H_m{}^{Bi} + c_p{}^{Bi} \left(T_m{}^{Bi} - T \right) + \frac{3}{2} c_p{}^{Te} \left(T_m{}^{Bi} - T \right) \right] \tag{2}$$

where M_{Bi}, $\Delta H_m{}^{Bi}$, $c_p{}^{Bi}$ and $c_p{}^{Te}$ are the molar mass, enthalpy of fusion and specific heats,

which are 209.0 g/mol, 11.3 kJ/mol, 25.7 J/mol-K and 25.4 J/mol-K respectively.

By comparing E_{melt} to the excess impact energy imparted, E^*, we find the impact energy

alone cannot explain all of the melting seen. I.e., under all experimental conditions $E^* < E_{melt}$.

For example at 300 K and an impact energy of 0.06 J, $E^* = 0.015$ J and $E_{melt} = 0.026$ J. We

can therefore say that under all of our experimental conditions, mechanically-induced melting

is not the only driving force for the reaction, and an additional source of energy is required to

explain the amount of reacted product. One logical explanation is that the heat of the Bi + Te

$\rightarrow$ Bi$_2$Te$_3$ reaction – which is measured by various authors to lie in the range 40 - 80

kJ/mol[34–36] and is thus comparable to the fusion enthalpy of Bi – is supplying some excess

thermal energy. Once triggered, the reaction energy could propagate the reaction further than

the impact energy alone would promote.

We now consider a reaction mechanism where such reaction heat is taken into account. The

amount of energy required to melt one mole of Bi$_2$Te$_3$ is

$$E_{melt,mol} = \Delta H_m{}^{Bi} + c_p{}^{Bi} \left(T_m{}^{Bi} - T \right) + \frac{3}{2} c_p{}^{Te} \left(T_m{}^{Bi} - T \right). \tag{3}$$

The number of Bi moles that can undergo melting from the excess impact energy, E^*, is

therefore

$$n_0 = \frac{E^*}{E_{melt,mol}}. \tag{4}$$

Once the n_0 moles of molten Bi have reacted with Te, they liberate the corresponding heat of

reaction, $n_0 \Delta H_r / 2$. This heat could then be used to melt further Bi, and so on in a cycle of

heat release and melting. The number of moles reacted, in the limit of no heat losses, in the i-th cycle of such release, would be:

$$n_i = n_0 \left(\frac{\Delta Hr/2}{E_{melt,mol}} \right)^i.$$ (5)

In the limit of infinite steps, the total number of moles melting, i.e. $n_{tot} = n_0 + n_1 + \ldots n_\infty$, is a geometric series, which converges to:

$$n_{tot} = \frac{E^*}{E_{melt,mol} - \Delta H_r/2}.$$ (6)

Equation (6) sets the upper limit for how much product can be formed using the impact energy and the heat of reaction. Fig. 4 compares this limit to the actual experimental values of product formation, on a plot of $E_{melt,mol}$ vs. E^*/n_{tot}. The line corresponding to equation (6) intercepts the y-axis at $\Delta H_r/2$, while equation (2) – i.e. the case where the reaction enthalpy is neglected – intercepts at the origin. All experimental data points lie well above equation (2), confirming that mechanically induced melting is not the only driving force. Furthermore, the data lie below equation (6), indicating that not all of the enthalpy of reaction is transferred into extra product being formed. The discrepancy between values predicted by equation (6) and those measured suggests that a considerable amount of heat is lost to the surroundings before it can induce further reaction. Indeed, synthesis of Bi_2Te_3 by self-propagating high temperature synthesis was recently demonstrated,[37] which corroborates the view that during milling, full propagation of the reaction to consume the entire charge must be prevented by heat loss.
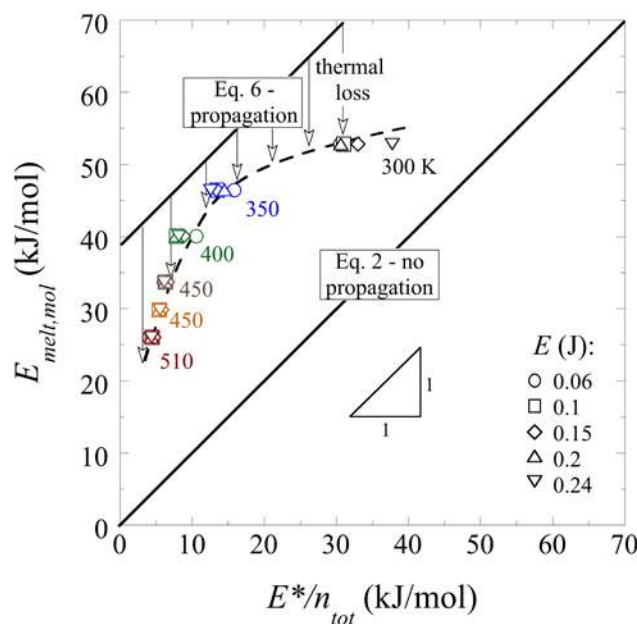
Figure 4 | The reaction is partially propagated by the enthalpy of mixing. The energy required to react product, $E_{melt,mol}$ is plotted as a function of energy supplied at impact, E^*/n_{tot}. All data lie well above equation (2), confirming that the impact energy alone cannot account for the amount of reaction, and thus the enthalpy of the Bi+Te→Bi$_2$Te$_3$ reaction (taken to be 79 kJ/mol[35]) must account for the extra product formed. The fact that the data lies below equation (6) indicates that such propagation is only partial, thus a significant portion of the reaction heat must be dissipated. The dashed line is drawn as a guide to the eye.

It is worthwhile noting that the reaction rate in this system is much faster than seen in conventional mechanochemical processes. The chemical conversion kinetics of this system are compared in Fig. 5 to the kinetics of other gradually mixing systems, processed under identical conditions, extracted from previous studies, e.g.[33] (shown as symbols), as well as some instantaneous MSRs (shown as vertical lines at the point of combustion[38]). The present system is one to two orders of magnitude faster than conventional gradually driven reactions. By comparison, MSRs proceed to completion in an instantaneous manner, although the energy requirement varies between about 1 and 10 kJ/g in general. We have also demonstrated that other powder mixtures can react similarly to Bi$_2$Te$_3$ mixtures: SnTe and PbTe (see Supplementary Notes 5-6 and Supplementary Table 1).

The fact that product forms so rapidly in the Bi + Te system may explain why the reaction does not self-propagate; the reaction is mostly complete at energy doses where typical MSRs tend to ignite, indicating that the microstructure is not significantly refined before the reactants become consumed. Similarly, the reaction Ti + C → TiC will usually occur as MSR, but when milled at sufficiently high intensities, a more local reaction can occur, thus preventing self-propagation from happening[39].
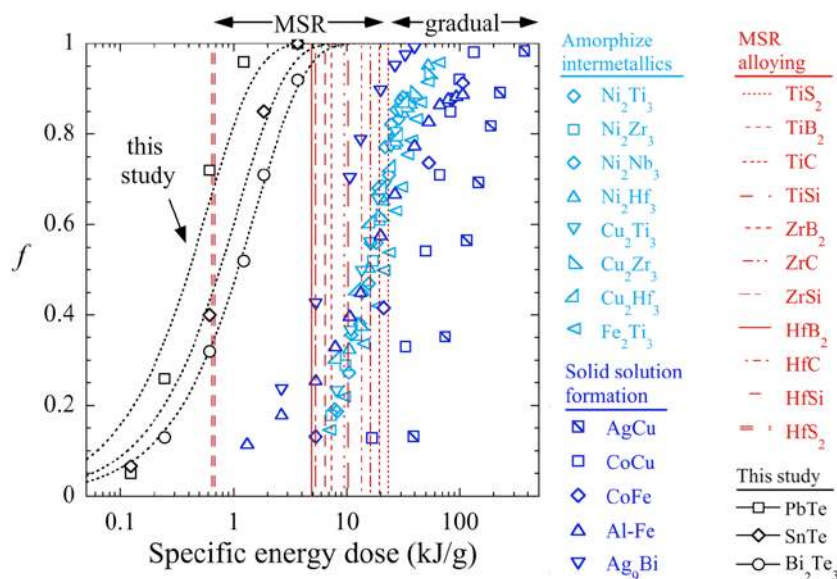

Figure 5 | The kinetics of phase formation are much faster than typical mechanochemical reactions. The kinetics of Bi_2Te_3 formation are compared to (i) self-propagating (MSR) systems (represented by vertical red lines), (ii) gradually reacting systems (blue symbols) [33,40–42] and (iii) similarly behaving melt-driven reactions, SnTe and PbTe. Compared to other gradual reactions Bi_2Te_3 is unusually rapid, e.g. the energy dose for 50% transformation is about 1 kJ/g for Bi_2Te_3 but between 10 and 100 kJ/g for the formation of solid solutions or amorphization of intermetallics. However it is kinetically distinct from instantaneous MSR reactions.

Molten phase reactions in other systems

The above microscopy and kinetic analyses together corroborate the view that molten Bi drives the abnormally fast mechanochemical reaction of Bi and Te. The additional analysis of the SnTe and PbTe systems in Supplemental Notes 5-6 shows that this phenomenon is not limited to a single system, but could be broadly applicable in a variety of materials. To elaborate the required conditions for molten phases in general mechanochemical processing

12

and other material systems, we perform here a simple estimate of the impact temperature during a milling collision. The impact temperature rise model by Schwarz and Koch[43] can be represented as: $\Delta T = \phi/e$, where e is the thermal effusivity of the powder being milled, and $\phi = \rho_b v^2 (4Rv_s/\pi)^{1/2}$ is parameter that is dependent on the milling conditions; R, ρ_b and v_s are parameters of the ball: radius, material density and velocity of sound respectively, while v is the impact velocity. Replacing the temperature rise with: $\Delta T = T - T_m$, and rearranging leads to the following expression:

$$\phi = e(T-T_m). \tag{7}$$

From the criterion of equation (7), it can be inferred that if $e(T - T_m)$ is below a critical value of φ set by the milling parameters, then the melting point should be reached during the collision process.

Fig. 6 shows a plot of thermal effusivity vs. $T - T_m$ for a range of metals and semimetals for which data was available[44]. The plot shows a broad variation in φ values for different materials; almost three orders of magnitude span between the most volatile element, Ga, and the most refractory element, W. Melting criteria are superimposed for different types of mechanochemical reactors[5,45], with different relative impact velocities, v: low energy, e.g. mortar and pestle (~0.25 m/s), horizontal rod- or attritor-type mills (~1 m/s); high energy ball mill, e.g. SPEX mill (~5 m/s); and even higher energy, e.g. Simoloyer mill (~10 m/s).

In Fig. 6, elements lying to the left of a line could reasonably exhibit melting if processed by the corresponding technique at room temperature, based on the estimated temperature rise of equation (7). The positioning of Bi in the bottom left corner of the diagram – i.e. low melting point and low thermal effusivity – is critical to understanding its unique mechanochemical behavior. The fact that it lies to the left of the SPEX mill line suggests melting is predicted to occur in Bi, along with other volatile elements such as Na, Li and K; these have incidentally

all been seen to react rapidly in high energy ball mills[46], which we may now suggest is associated with melting. Te is similarly positioned with Bi, suggesting it can melt also, but we suggest that Te's factor-of-three higher hardness[47] means that Bi deforms preferentially over Te, and thus governs the overall reactivity.

It is interesting to note that some other elements commonly processed by high energy ball milling lie to the left of the v=10 m/s line, such as Sn, Cd, Pb, and In. The sulphides, selenides and tellurides of those elements are known to react in a self-sustaining manner under low-energy milling[48]. However, their placement here suggests these elements could undergo melting if processed under sufficiently aggressive conditions. We have indeed observed such a transition from self-sustaining to gradual mixing in SnTe and PbTe powder mixtures, and this is compounded by observations of molten phases (see Supplementary Notes 5-6). These and other metal-chalcogen compounds have functional properties with important optical, thermoelectric, and photovoltaic applications, and powder milling processes have been proposed as synthesis pathways for several such compounds[49]. Our identification of a threshold of milling intensity to form these compounds rapidly by melt-assisted mechanochemical synthesis offers new insight into process design for such compounds.
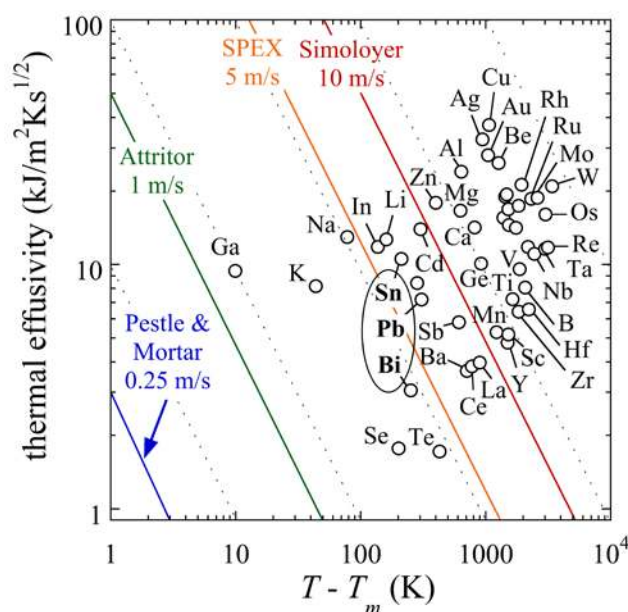
Figure 6 | Other elements that could melt under mechanochemical processing. The tendency of an element to melt during impact is represented by the criterion of equation (7): $\phi = e(T - T_m)$, which is plotted for several types of mechanochemical reactor. Bi lies to the left of the $v = 5$ m/s line, predicting melting will occur in a SPEX mill, in agreement with this study. The presence of other elements within the outlined processing space, suggests they could exhibit melt-driven transformations, particularly when processed under very aggressive ($v > 5$ m/s) conditions.

Outlook

With the present elaboration of a melt-driven mechanochemical reaction, it is hoped that this reaction pathway can be sought in many other systems. Thermal effects at the collision site are usually neglected in mechanochemical theories of mixing, and there is therefore scope for improved models. From an engineering viewpoint, this study offers potential guidance for rapid synthesis of functional compounds, many of which comprise one or more of the volatile elemental components that we predict are conducive to melt-driven mechanochemical reaction.

References

1. Hickenboth, C. R. *et al.* Biasing reaction pathways with mechanical force. *Nature* **446,** 423–427 (2007).
2. Seidel, C. A. M. & Kühnemuth, R. Mechanochemistry: Molecules under pressure. *Nat. Nanotechnol.* **9,** 164–165 (2014).
3. Sawyer, W. G., Argibay, N., Burris, D. L. & Krick, B. A. Mechanistic Studies in Friction and Wear of Bulk Materials. *Annu. Rev. Mater. Res.* **44,** 395–427 (2014).
4. Pastewka, L., Moser, S., Gumbsch, P. & Moseler, M. Anisotropic mechanical amorphization drives wear in diamond. *Nat. Mater.* **10,** 34–38 (2011).
5. Suryanarayana, C. Mechanical alloying and milling. *Prog. Mater. Sci.* **46,** 1–184 (2001).
6. James, S. L. *et al.* Mechanochemistry: opportunities for new and cleaner synthesis. *Chem. Soc. Rev.* **41,** 413–447 (2012).
7. Friščić, T. *et al.* Real-time and in situ monitoring of mechanochemical milling reactions. *Nat. Chem.* **5,** 66–73 (2013).
8. Katsenis, A. D. *et al.* In situ X-ray diffraction monitoring of a mechanochemical reaction reveals a unique topology metal-organic framework. *Nat. Commun.* **6,** (2015).
9. Baláž, P. & Dutková, E. Fine milling in applied mechanochemistry. *Miner. Eng.* **22,** 681–694 (2009).
10. McCormick, P. G. & Froes, F. H. The fundamentals of mechanochemical processing. *JOM* **50,** 61–65 (1998).
11. Baláž, P. *et al.* Hallmarks of mechanochemistry: from nanoparticles to technology. *Chem. Soc. Rev.* **42,** 7571–7637 (2013).
12. Valiev, R. Nanostructuring of metals by severe plastic deformation for advanced properties. *Nat. Mater.* **3,** 511–516 (2004).
13. Xu, J., Herr, U., Klassen, T. & Averback, R. S. Formation of supersaturated solid solutions in the immiscible Ni–Ag system by mechanical alloying. *J. Appl. Phys.* **79,** 3935–3945 (1996).
14. Gente, C., Oehring, M. & Bormann, R. Formation of thermodynamically unstable solid solutions in the Cu-Co system by mechanical alloying. *Phys. Rev. B* **48,** 13244–13252 (1993).
15. Han, B. Q., Ye, J., Tang, F., Schoenung, J. & Lavernia, E. J. Processing and behavior of nanostructured metallic alloys and composites by cryomilling. *J. Mater. Sci.* **42,** 1660–1672 (2007).
16. Martin, G. & Bellon, P. Driven alloys. *Solid State Phys.* **50,** 189–331 (1996).
17. Lund, A. C. & Schuh, C. A. Driven Alloys in the Athermal Limit. *Phys. Rev. Lett.* **91,** 235505 (2003).
18. Odunuga, S., Li, Y., Krasnochtchekov, P., Bellon, P. & Averback, R. S. Forced Chemical Mixing in Alloys Driven by Plastic Deformation. *Phys. Rev. Lett.* **95,** 045901 (2005).
19. Vo, N. Q., Odunuga, S., Bellon, P. & Averback, R. S. Forced chemical mixing in immiscible alloys during severe plastic deformation at elevated temperatures. *Acta Mater.* **57,** 3012–3019 (2009).
20. Ashkenazy, Y., Vo, N. Q., Schwen, D., Averback, R. S. & Bellon, P. Shear induced chemical mixing in heterogeneous systems. *Acta Mater.* **60,** 984–993 (2012).
21. Xu, J., He, J. H. & Ma, E. Effect of milling temperature on mechanical alloying in the immiscible Cu-Ta system. *Metall. Mater. Trans. A* **28,** 1569–1580 (1997).
22. Koch, C. C. The Synthesis of Non-Equilibrium Structures by Ball-Milling. *Mater. Sci. Forum* **88-90,** 243–262 (1992).
23. Benjamin, J. S. Fundamentals of Mechanical Alloying. *Mater. Sci. Forum* **88-90,** 1–18 (1992).
24. Takacs, L. Self-sustaining reactions induced by ball milling: An overview. *Int. J. Self-Propagating High-Temp. Synth.* **18,** 276–282 (2010).
25. Takacs, L. Self-sustaining reactions induced by ball milling. *Prog. Mater. Sci.* **47,** 355–414 (2002).
26. Maurice, D. R. & Courtney, T. H. The physics of mechanical alloying: A first report. *Metall. Trans. A* **21,** 289–303 (1990).

27. Lewandowski, J. J. & Greer, A. L. Temperature rise at shear bands in metallic glasses. *Nat. Mater.* **5,** 15–18 (2006).
28. Bowden, F. P. & Persson, P. A. Deformation, Heating and Melting of Solids in High-Speed Friction. *Proc. R. Soc. Lond. Ser. Math. Phys. Sci.* **260,** 433–458 (1961).
29. Gerasimov, K. B. & Boldyrev, V. V. On mechanism of new phases formation during mechanical alloying of Ag-Cu, Al-Ge and Fe-Sn systems. *Mater. Res. Bull.* **31,** 1297–1305 (1996).
30. Urakaev, F. K. & Boldyrev, V. V. Mechanism and kinetics of mechanochemical processes in comminuting devices: 1. Theory. *Powder Technol.* **107,** 93–107 (2000).
31. Delogu, F. A possible alloying mechanism in idealized collisions between Cu and Sn crystals. *Chem. Phys. Lett.* **521,** 125–129 (2012).
32. Delogu, F. & Cocco, G. Crystallite size refinement in elemental species under mechanical processing conditions. *Mater. Sci. Eng. A* **422,** 198–204 (2006).
33. Delogu, F., Schiffini, L. & Cocco, G. The invariant laws of the amorphization processes by mechanical alloying. *Philos. Mag. A* **81,** 1917–1937 (2001).
34. Morgant, G., Feutelais, Y., Legendre, B., Castanet, R. & Coulet, A. Themodynamic behaviour of Bi-Te alloys. *Z. Fuer Met. Res. Adv. Tech.* **81,** 44–48 (1990).
35. Misra, S. & Bever, M. B. On the solid solutions of bismuth telluride and bismuth selenide. *J. Phys. Chem. Solids* **25,** 1233–1241 (1964).
36. Humphry-Baker, S. A. & Schuh, C. A. The nanocrystalline thermoelectric compound Bi2Te3 forms by a particle-wise explosive reaction during mechanical alloying. *Scr. Mater.* **65,** 516–519 (2011).
37. Su, X. *et al.* Self-propagating high-temperature synthesis for compound thermoelectrics and new criterion for combustion processing. *Nat. Commun.* **5,** 4908 (2014).
38. Takacs, L. Ball Milling-Induced Combustion in Powder Mixtures Containing Titanium, Zirconium, or Hafnium. *J. Solid State Chem.* **125,** 75–84 (1996).
39. Delogu, F. & Takacs, L. Mechanochemistry of Ti–C powder mixtures. *Acta Mater.* **80,** 435–444 (2014).
40. Musu, E., Mura, G., Ligios, G. & Delogu, F. Formation of metastable solid solutions by mechanical alloying of immiscible Ag and Bi. *J. Alloys Compd.* **576,** 80–85 (2013).
41. Delogu, F. & Cocco, G. Kinetics of structural evolution in immiscible Ag-Cu and Co-Cu systems under mechanical processing conditions. *Mater. Sci. Eng. A* **402,** 208–214 (2005).
42. Delogu, F. Kinetics of allotropic phase transformation in cobalt powders undergoing mechanical processing. *Scr. Mater.* **58,** 126–129 (2008).
43. Schwarz, R. B. & Koch, C. C. Formation of amorphous alloys by the mechanical alloying of crystalline powders of pure metals and powders of intermetallics. *Appl. Phys. Lett.* **49,** 146 (1986).
44. Shackelford, J. F. & Alexander, W. *CRC materials science and engineering handbook*. (CRC Press, 2001).
45. M. Abdellaoui, E. G. The physics of mechanical alloying in a modified horizontal rod mill: Mathematical treatment. *Acta Mater.* **44,** 725–734 (1996).
46. Monagheddu, M., Doppiu, S. & Cocco, G. MSR Reduction of Hexachlorobenzene. *J. Mater. Synth. Process.* **8,** 295–300 (2000).
47. ASM Handbook Volume 2: Properties and Selection: Nonferrous Alloys and Special-Purpose Materials - ASM International. at <http://www.asminternational.org/materials-resources/results/-/journal_content/56/10192/06182G/PUBLICATION>
48. Tschakarov, C. G., Gospodinov, G. G. & Bontschev, Z. Über den Mechanismus der mechanochemischen Synthese anorganischer Verbindungen. *J. Solid State Chem.* **41,** 244–252 (1982).
49. Ramasamy, K., Malik, M. A., Revaprasadu, N. & O'Brien, P. Routes to Nanostructured Inorganic Materials with Potential for Solar Energy Applications. *Chem. Mater.* **25,** 3551–3569 (2013).
50. Delogu, F., Mulas, G., Schiffini, L. & Cocco, G. Mechanical work and conversion degree in mechanically induced processes. *Mater. Sci. Eng. A* **382,** 280–287 (2004).

Methods

Materials

Powders of Bi and Te with a nominal purity of 99.99% and 99.8% respectively, and mesh sizes of -100 and -200 respectively, were weighed according to the stoichiometry Bi_2Te_3. All handling of the powders was performed inside a glove box under high-purity argon atmosphere, with less than 2 ppm oxygen, nitrogen and water vapor (see Supplementary Note 1).

Impact observations

A SPEX 8000 mill was used with a standard stainless steel flat ended milling vial with a single 8g ball and approximately 10g of powder. The mill was operated at an impact frequency of 35.3Hz, at which speed the ball velocity is calculated to be 5.1 m/s [33,50] (see Supplementary Note 2), and the corresponding kinetic energy of each collision is E=0.103 J, which is thus directly comparable to the impact energies achieved in the ball-drop reactor. Note that the term 'impact energy' does not pertain to the deformation mode of individual powder particles but rather to the macroscale motion of the milling ball relative to the vial. The mill was operated for approximately 8 seconds, which yielded about 150 collisions at each end of the vial. 23 individual powder compacts that adhered to the vial surface and that had unambiguously undergone only a single collision were imaged and analysed stereographically using the point counting method. Images were taken inside a 6610 LV scanning electron microscope operated at 20 kV in back-scattered imaging mode.

Kinetic analysis via ball-drop reactor

The reactor geometry was a cylinder roughly 20 cm in height, and 2 cm in diameter, with a rounded bottom base and stainless steel construction (Fig. 2a). Each milling experiment was prepared by adding to the reactor a single milling ball (also of stainless steel) of 20 g, 3 g of powders mixed according to Bi_2Te_3 stoichiometry, and sealed in Ar atmosphere. Milling was

performed by attaching the reactor to a mechanical arm that subjected it to a harmonic

oscillation of 5 s period along the vertical axis. The collision amplitude was varied to allow

collision energies between about 0.06 and 0.24 J. The temperature of this reactor was actively

controlled between 300 and 510 K using a metallic heating jacket. During each experiment

the number of collisions, n, was recorded, after which the 3g of powders were removed for

characterisation and the reactor refilled. The degree of phase transformation, i.e. $2Bi + 3Te$

$\rightarrow Bi_2Te_3$, in the as-milled powders was characterized by XRD, using a Rigaku DMax/A

diffractometer with a Cu K_α radiation source. All scans were collected over a scan range of

15 to 80 degrees 2θ, in discrete step mode with angular displacements of 0.05 degrees at a

rate of 20 s per step (see Supplementary Note 3). Pattern intensity was fitted using the

Rietveld method to extract relative phase fractions of Bi, Te and Bi_2Te_3. Raw data from these

fits is provided in Supplementary Note 1.

Author contributions

F.D., S.G. and S.H-B. designed and performed experiments; F.D., C.S. and S. H-B. analysed the data and co-wrote the manuscript.

Competing financial interests

The authors declare no competing financial interests.

Melt-driven mechanochemical phase transformations in moderately exothermic powder mixtures

Samuel A. Humphry-Baker*[1,2], Sebastiano Garroni[3], Francesco Delogu[4] and Christopher A. Schuh[1]

[1]*Department of Materials Science and Engineering, Massachusetts Institute of Technology, Cambridge, MA 02139, USA*

[2]*Department of Materials, Imperial College, London SW7 2AZ, UK*

[3]*Dipartimento di Chimica e Farmacia, Università degli Studi di Sassari, via Vienna 2, 07100 Sassari, Italy*

[4]*Dipartimento di Ingegneria Meccanica, Chimica e dei Materiali, Università degli Studi di Cagliari, via Marengo 2, 09123 Cagliari, Italy*

* Corresponding author email: shumphry@ic.ac.uk

Supplementary Note 1. Starting powders

To avoid oxidation, storage and handling of powders were performed in a glove box under high purity argon atmosphere, with oxygen and humidity levels below 2 ppm. Supplementary Figure 1 shows images of the starting powders taken in a Scanning Electron Microscope (SEM) under secondary electron mode. The average particle sizes of the powders were determined to be about 15, 3, 11 and 14 μm for Bi, Sn, Pb and Te respectively.
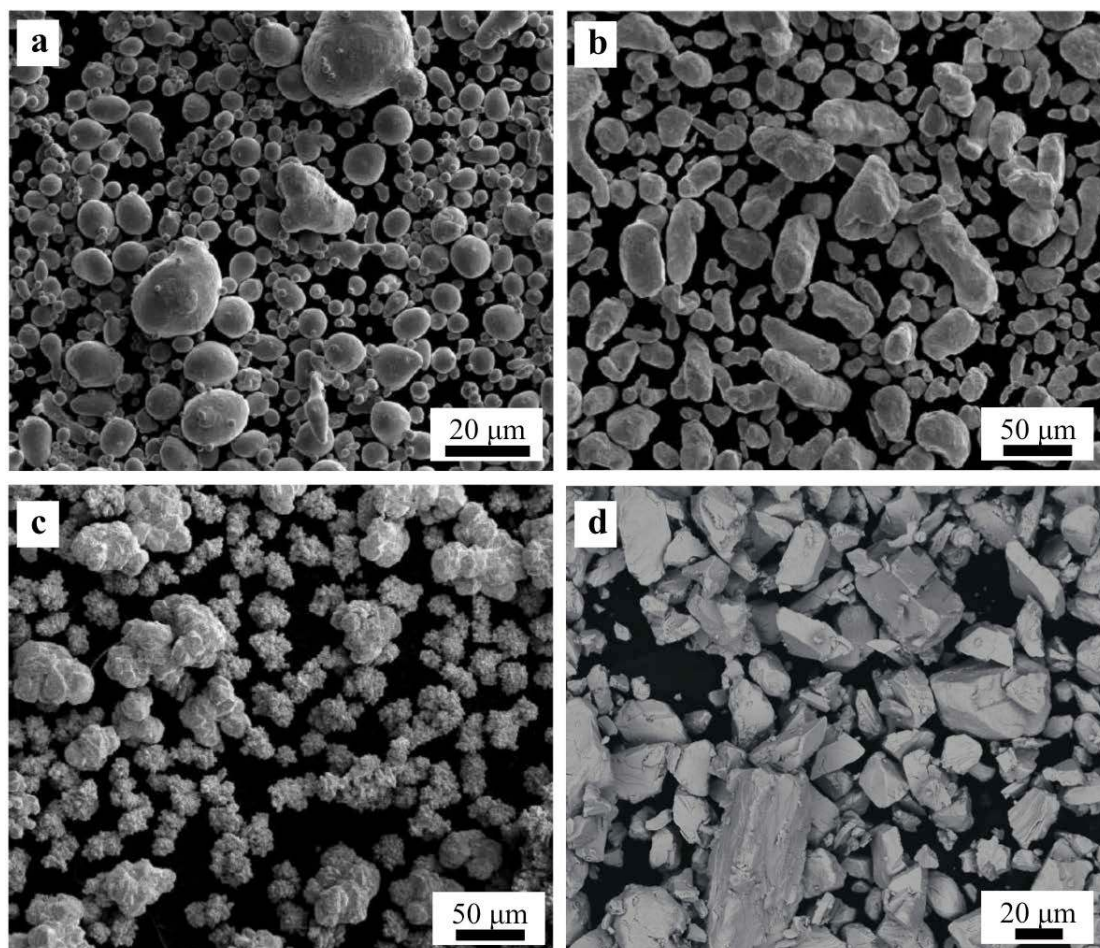
Supplementary Figure 1 | As-received powder particles. SEM images taken in secondary electron mode: **a.** Sn, **b.** Pb, **c.** Te, and **d.** Bi.

Supplementary Note 2. Impact velocity in the SPEX mill

Milling experiments were performed in a SPEX Mixer/Mill 8000 working at a frequency of vial motion between approximately 730 and 1200 min^{-1}. For all experiments, a flat-ended milling vial was used, which was made from stainless steel and had an internal volume of 65 ml. The vial was loaded with a single 8 g ball and between 2 and 10 g of elemental powders, weighed according to the stoichiometry of the target intermetallic compounds. The velocity of each impact was estimated from the time-lag between the vial reaching its oscillation extremity, and the impact between ball and vial. To obtain the time-lag measurement the vial motion was monitored using a magnetic proximity sensor, and the collision dynamics registered using a piezoelectric sensor. These methods are explained in detail elsewhere,[51–53] however we show examples of these signal measurements in Supplementary Figure 2 for cases with and without powder charge. In the specific case of a powder charge larger than 1.5 g and a frequency of 1100 min^{-1}, the impact velocity is determined to be approximately 5.1 m s^{-1}.
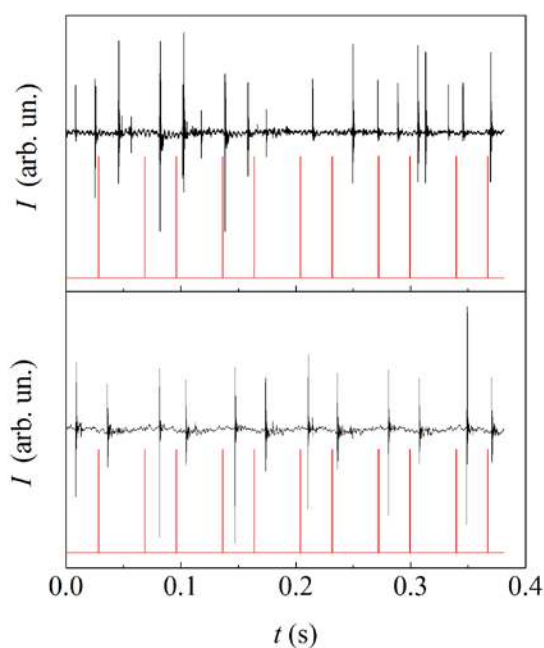
Supplementary Figure 2 | Collision sequences in the SPEX mill. Red is the magnetic proximity signal, showing a peak every half-cycle of oscillation. Black is the piezoelectric signal, showing a peak every ball-vial collision. **a.** With no powder in the vial, a highly disordered collision sequence is observed with large variability in lag times between oscillation and collision. **b.** With 10 g of powder, a regular and repeatable collision sequence with smaller variability in lag times emerges, allowing a clean estimation of the dominant impact velocity.

Supplementary Note 3. Treatment of X-ray diffraction patterns.

X-ray diffraction (XRD) analyses were carried out on disk-shaped specimens of powders compacted at about 1 bar. Occasionally, narrow 2θ ranges were studied in greater detail to clarify specific features of the peak profiles. A typical Rietveld fit of the experimental data – as used to determine the relative volume fractions of each phase – is shown in Supplementary Figure 3. The high quality of fit indicates the lack of any amorphous phase – as would otherwise be present by a low angle 'hump'. To further confirm the lack of an amorphous phase, a similar analysis was performed on powders subjected to extended milling treatments – up to specific energy doses on the order of 10^5 J g^{-1}, i.e. about two orders of magnitude greater than the largest treatment reported in this study. Even in the most heavily deformed cases no amorphous hump could be detected.
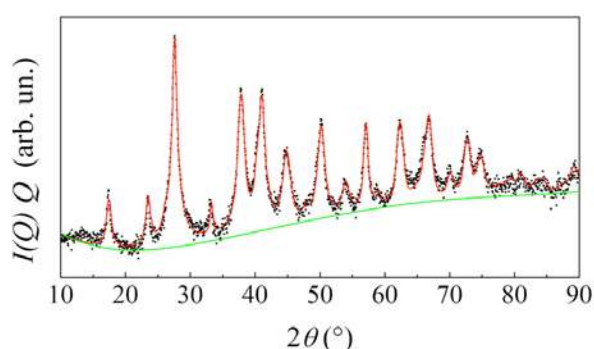
Supplementary Figure 3 | A typical XRD pattern of Bi$_{40}$Te$_{60}$ powder mixtures together with the best-fitted Rietveld integral profile. The raw XRD data is shown as black dots, the best-fitted profile in red and the background in green. The small deviation between the data and Rietveld profile indicates a high quality of fit.

Supplementary Note 4. Melting point depression in Bi.

In order to investigate the effect of pressure on the melting point of Bi, we estimate the maximum shear strain rate that could be experienced during a typical collision between a ball

and the vial as: [54] $\dot{\gamma} = v/Mh$, where v is the impact velocity, h is the initial height of the trapped powder compact and M is the Taylor factor. Using the values of $v = 5$ m s^{-1}, $h = 100$ μm and $M = 3$, which are typical for SPEX mill, $\dot{\gamma} \approx 2 \times 10^4 \, s^{-1}$. At plastic strain rates of this magnitude, deformation becomes limited by phonon drag. [55] Here, we note that the following empirical law is generally obeyed for the shear stress of most metals: [55]

$$\tau = \dot{\gamma} * \mu/5 \times 10^6$$

where μ the shear modulus (12 GPa for Bi). These values predict a stress of $\tau = 50$ MPa, which also corresponds to a hydrostatic stress of the same order. This hydrostratic stress is the driving force for any melting point depression, which is measured to be 38[56] or 39[57] K/GPa, giving an upper bound for melting point depression of about 2 K. For such a 2 K depression in melting point, the total energy required to melt 1 mol of Bi at 300 K, as given by Eq. 2, would be changed by about 0.1 %. We therefore neglect melting point depression in our analysis.

Supplementary Note 5. Evidence of molten reaction in other materials systems.

The following exothermic powder mixtures were investigated under high and low energy milling: $Pb_{50}Te_{50}$, $Sn_{50}Te_{50}$, $Ti_{70}C_{30}$ and $Zr_{70}C_{30}$. Milling experiments were performed in a ball-drop reactor, and in a SPEX mill 8000 approximately between 1000 and 1200 min^{-1} for

high intensity and between 730 and 800 min⁻¹for low intensity. The following evidence for a molten-phase reaction was found:

1) In the ball-drop reactor, cold-welded compacts of PbTe and SnTe appear to have melted and flowed as a liquid, see Supplementary Figure 4(a, c). At higher magnification, such compacts appear to show microstructures that are typical of casting solidification, which are impossible to achieve through mechanical deformation alone, see Supplementary Figure 4(b, d).
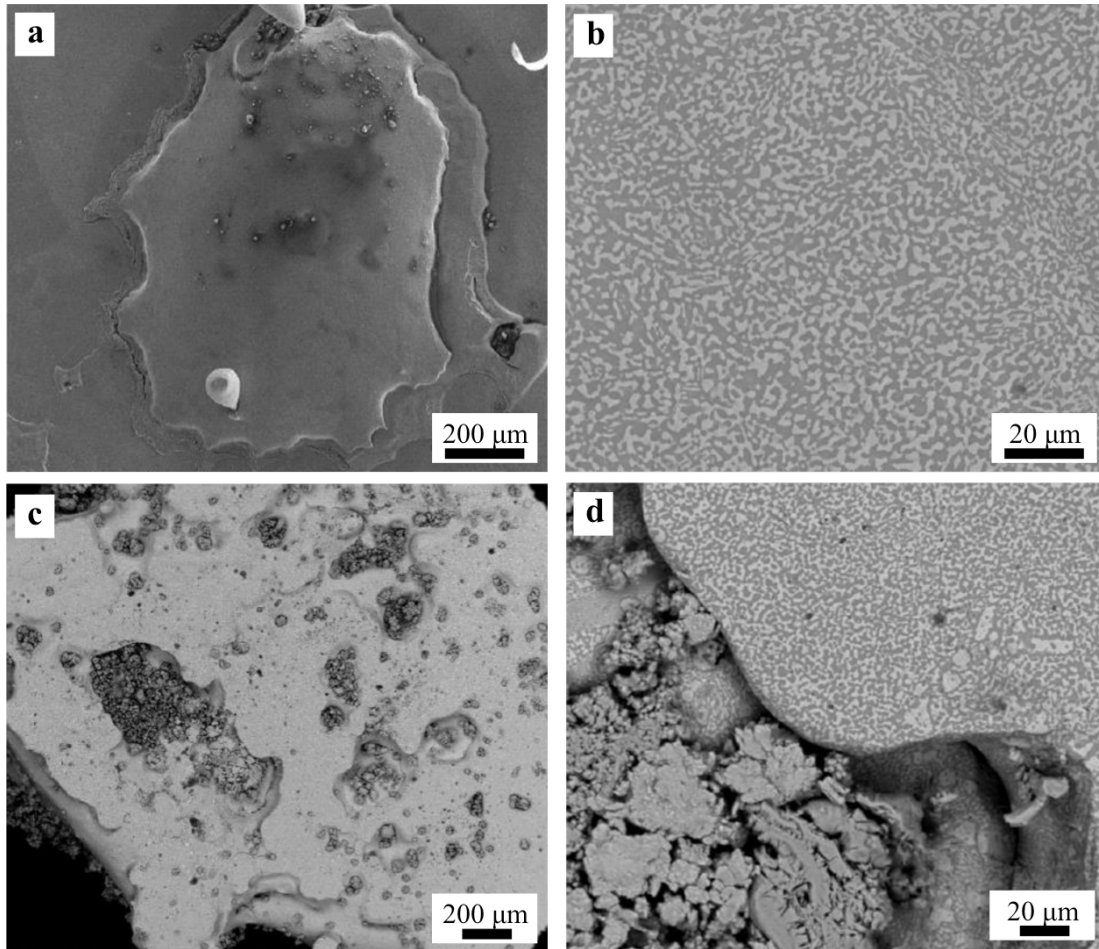
Supplementary Figure 4 | Evidence of molten phase reaction after ball-drop experiments on PbTe and SnTe powder mixtures. a. SEM image of PbTe compact at low magnification; **b**. PbTe at high magnification; **c**. SnTe at low magnification; **d**. SnTe at high magnification. At low magnifications compacts have rounded shapes indicating they have melted and evolved under the influence of surface tension. At high magnifications the microstructures appear similar to those of the corresponding cast metal.

2) Under SPEX high-energy milling, splashes and veins, suggestive of local melting processes, are seen in PbTe and SnTe (see Supplementary Figure 5).
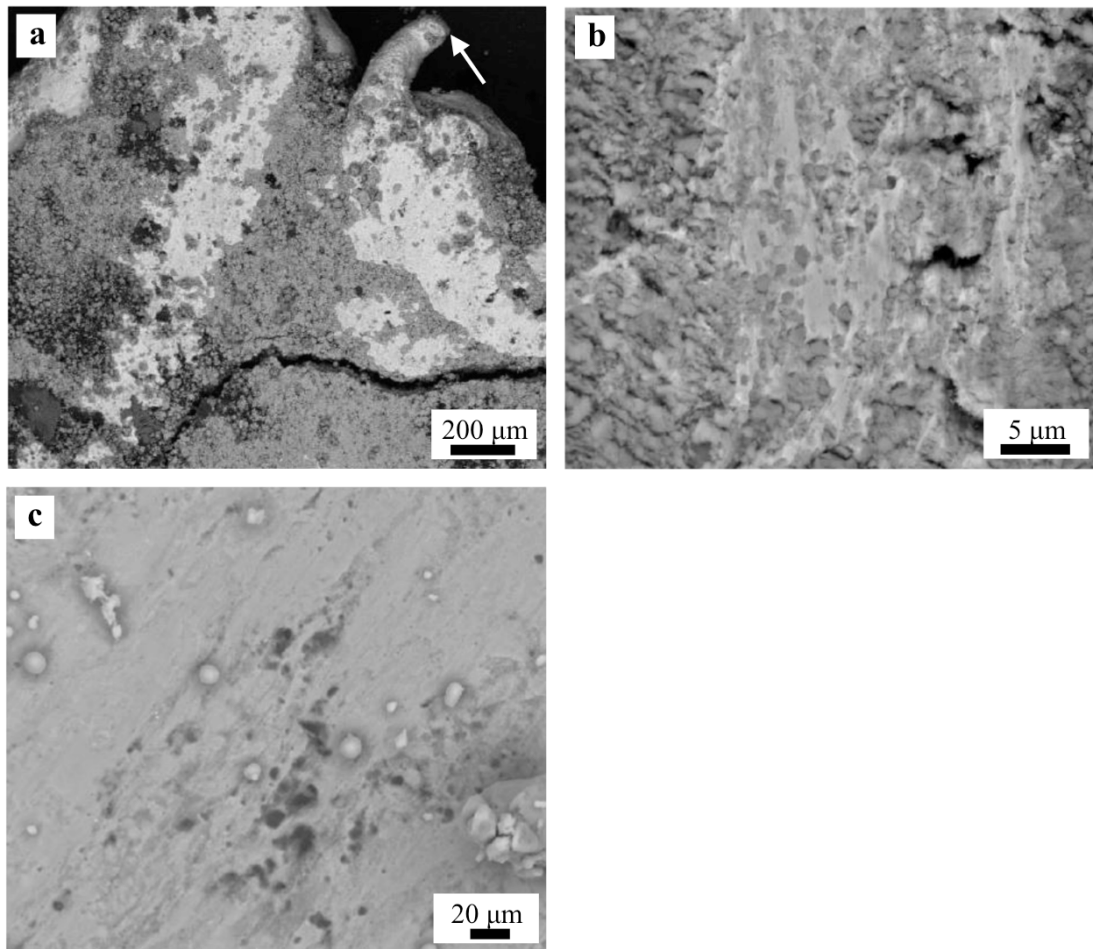
Supplementary Figure 5 | Evidence of molten phase reaction after ball-drop experiments on PbTe powder mixtures. a. SEM image of one compact where a liquid filament has been ejected from the compact periphery (indicated by arrow) **b and c**. higher magnification images of liquid veins, splashes and droplets forming on the compact surface.

3) Under SPEX high-energy milling, the chemical conversion kinetics are gradual (see Supplementary Table 1 and graphically illustrated in Supplementary Figure 6) and can be best-fitted with the same exponential kinetic law reported in the manuscript for $Bi_{40}Te_{60}$ mixtures, meaning that the reaction is similarly initiated instantaneously from the very first collision. This mechanistic picture runs counter to conventional mechanical alloying reactions, which tend to exhibit sigmoidal kinetic trends, suggesting the occurrence of a molten-phase reaction. Furthermore, the conversion processes in all of these powders are about one to two orders of magnitude faster than conventional mechanical alloying processes, and are particularly rapid (i.e. similar in magnitude to $Bi_{40}Te_{60}$) in the case of $Pb_{50}Te_{50}$ and $Sn_{50}Te_{50}$, presumably because Pb and Sn are easily melted, like Bi, and thus the amount of reacted material in each

collision is extensive.
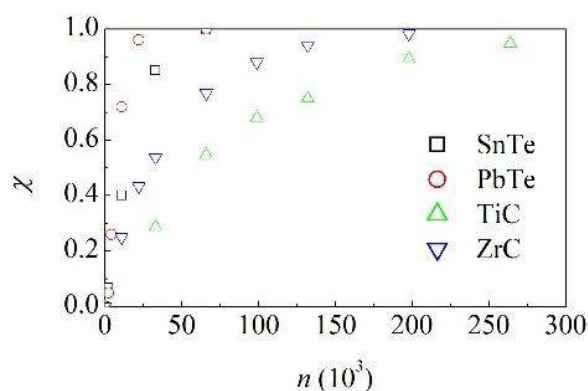
Supplementary Figure 6 | Rapid conversion kinetics with exponential kinetic trends are observed for Pb$_{50}$Te$_{50}$, Sn$_{50}$Te$_{50}$, Ti$_{70}$C$_{30}$ and Zr$_{70}$C$_{30}$. Such kinetic trends are indicative of a local reaction driven by the presence of molten phase.

Supplementary Table 1. SPEX mill kinetic data on other material systems.

n = represents number of collisions (x 10^3); f = volume fraction of intermetallic phase

Pb$_{50}$Te$_{50}$		Sn$_{50}$Te$_{50}$		Bi$_{60}$Te$_{60}$		Ti$_{70}$C$_{30}$		Zr$_{70}$C$_{30}$	
n	f	n	f	n	f	n	f	n	f
0	0	1	0	0	0	33	0.286	11	0.25
2.2	0.05	2	0.066	2	0.13	66	0.545	22	0.432
4.4	0.26	5	0.4	5	0.32	99	0.679	33	0.537
11	0.72	15	0.85	10	0.52	132	0.749	66	0.769
22	0.96	20	1	15	0.71	198	0.891	99	0.88
66	1			30	0.92	264	0.948	132	0.941
								198	0.982

4) NB: Under low intensity milling, SnTe and PbTe exhibited exhibit self-propagating reactions, indicating that if enough product is formed, such a reaction could be followed by an autocatalytic reaction that consumes the entire powder charge.

Supplementary Note 6. Molten droplet experiments.

To understand some of the structures observed during milling in the SnTe and PbTe systems, an experiment was performed where droplets of molten Sn or Pb were dropped into a bed of Te powder. The experiments were performed under pure Argon. Upon droplet impact,

incandescence was observed, indicating a vigorous reaction between the Sn/Te and Pb/Te mixtures. The reacted areas were imaged under SEM and compared to the powder morphologies from milling experiments. The morphologies from both droplets and milling are indistinguishable in nature (see Supplementary Figure 7) indicating that molten phases must be involved in the reaction. For brevity we show the case of SnTe, however the morphologies for PbTe are remarkably similar.
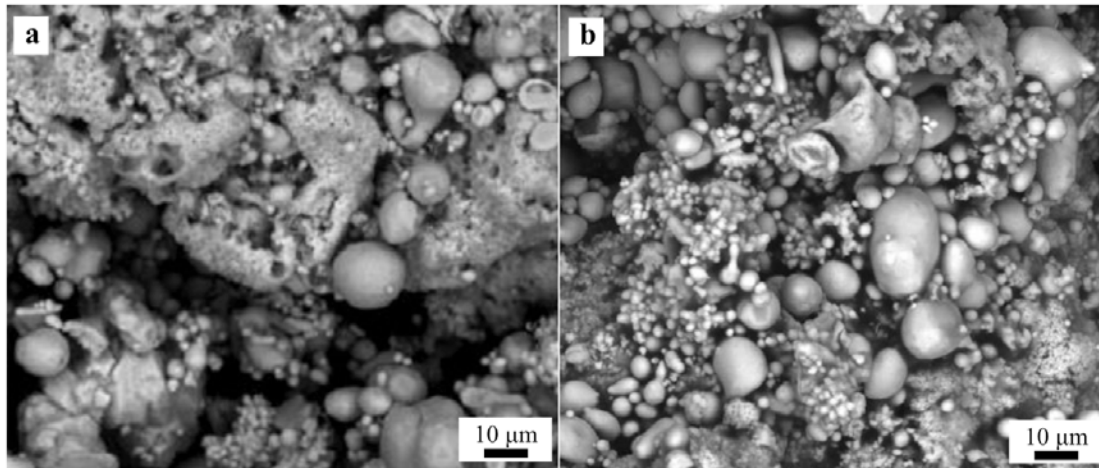
Supplementary Figure 7 | SEM images of SnTe powder mixtures after molten droplet and milling experiments appear indistinguishable. a. milling experiment **b**. molten droplet experiment. The morphologies indicate that melting occurs during milling of SnTe powder mixtures.

Supplementary Table 2. Ball-drop reactor kinetic data on Bi-Te mixtures.

n = number of collisions (x 10^3); f = volume fraction of intermetallic phase

Temperature, T (K)											
300		**350**		**400**		**450**		**480**		**510**	
n	f	n	f	n	f	n	f	n	f	n	f
2	0.25	1	0.366	0.3	0.216	0.3	0.451	0.3	0.538	0.1	0.314

29

	x	val	x	val	x	val	x	val	x	val	x	val
0.06	4	0.384	2	0.609	0.6	0.404	0.6	0.699	0.6	0.774	0.2	0.529
	6	0.542	3	0.742	0.9	0.5	0.9	0.839	0.9	0.896	0.3	0.677
	8	0.668	4	0.853	1.2	0.622	1.2	0.917	1.2	0.946	0.6	0.896
	10	0.727	5	0.901	1.5	0.685	1.5	0.952	1.5	0.977	0.9	0.966
	12	0.768	6	0.934	1.8	0.768	1.8	0.974				
	14	0.838	7	0.966	2.1	0.818						
	16	0.853	8	0.975	2.4	0.838						
	18	0.904	9	0.985	2.7	0.888						
					3	0.931						
					3.3	0.913						
0.1	1	0.37	0.25	0.279	0.1	0.256	0.1	0.311	0.1	0.37	0.05	0.252
	2	0.614	0.5	0.483	0.2	0.368	0.2	0.515	0.2	0.601	0.1	0.44
	4	0.852	1	0.733	0.3	0.5	0.3	0.662	0.3	0.735	0.2	0.688
	6	0.936	1.5	0.87	0.4	0.645	0.4	0.773	0.4	0.842	0.3	0.825
	8	0.977	2	0.935	0.5	0.668	0.5	0.844	0.5	0.892	0.4	0.902
	10	0.991	2.5	0.96	0.6	0.75	0.6	0.884			0.5	0.945
	12	0.996	3	0.982	0.7	0.82	0.7	0.923			0.6	0.969
					0.8	0.839	0.8	0.946				
					0.9	0.89						
					1	0.933						
					1.1	0.952						
					1.2	0.947						
0.15	0.5	0.351	0.1	0.208	0.1	0.31	0.1	0.425	0.1	0.481	0.05	0.343
	1	0.577	0.2	0.373	0.2	0.524	0.2	0.665	0.2	0.727	0.1	0.564
	1.5	0.716	0.3	0.508	0.3	0.671	0.3	0.81	0.3	0.86	0.2	0.814
	2	0.813	0.4	0.607	0.4	0.773	0.4	0.891	0.4	0.932	0.3	0.92
	4	0.967	0.5	0.684	0.5	0.843	0.5	0.933	0.5	0.962	0.4	0.97
			1	0.903	1	0.975					0.5	0.985
0.2	0.5	0.487	0.1	0.261	0.1	0.446	0.05	0.324	0.05	0.384	0.05	0.451
	1	0.741	0.2	0.456	0.2	0.693	0.1	0.554	0.1	0.61	0.1	0.698
	1.5	0.873	0.3	0.604	0.3	0.83	0.15	0.698	0.15	0.766	0.15	0.834
	2	0.933	0.4	0.714	0.4	0.906	0.2	0.797	0.2	0.847	0.2	0.912
	2.5	0.961	0.5	0.791	0.5	0.948	0.25	0.864	0.25	0.908	0.25	0.952
	3	0.983	1	0.954								
0.24	0.252	0.348	0.1	0.361	0.1	0.501	0.05	0.384	0.05	0.424	0.02	0.271
	0.5	0.581	0.2	0.581	0.2	0.751	0.1	0.63	0.1	0.678	0.04	0.42
	0.752	0.733	0.3	0.733	0.3	0.876	0.15	0.767	0.15	0.809	0.06	0.561
	1	0.824	0.4	0.823	0.4	0.938	0.2	0.864	0.2	0.894	0.08	0.686
	1.252	0.882			0.5	0.969	0.25	0.914	0.25	0.939	0.1	0.765
	1.5	0.926									0.12	0.843
	2	0.969									0.14	0.868
											0.16	0.882
											0.18	0.926
											0.2	0.926
											0.22	0.978
											0.24	0.969
											0.26	0.977
											0.28	0.983

Supplementary References.

51. Cocco, G., Delogu, F. & Schiffini, L. Toward a Quantitative Understanding of the Mechanical Alloying Process. *J. Mater. Synth. Process.* **8,** 167–180 (2000).

52. Delogu, F., Schiffini, L. & Cocco, G. The invariant laws of the amorphization processes by mechanical alloying. *Philos. Mag. A* **81,** 1917–1937 (2001).

53. Delogu, F., Monagheddu, M., Mulas, G., Schiffini, L. & Cocco, G. Impact characteristics and mechanical alloying processes by ball milling: experimental evaluation and modelling outcomes. *Int. J. Non-Equilib. Process.* **11,** 235–269 (2000).

54. Maurice, D. R. & Courtney, T. H. The physics of mechanical alloying: A first report. *Metall. Trans. A* **21,** 289–303 (1990).

55. *Deformation-Mechanism Maps: The Plasticity and Creep of Metals and Ceramics*. (Pergamon Press, 1982).

56. mBridgman, P. W. Polymorphism, Principally of the Elements, up to 50,000 kg/cm^2. *Phys. Rev.* **48,** 893–906 (1935).

57. Yoon, W., Paik, J. S., LaCourt, D. & Perepezko, J. H. The effect of pressure on phase selection during nucleation in undercooled bismuth. *J. Appl. Phys.* **60,** 3489–3494 (1986).